

RESEARCH ARTICLE

Open Access



# Sulfur-doped carbon dots synthesis under microwave irradiation as turn-off fluorescent sensor for Cr(III)

Siti Raudhatul Kamali<sup>1,2</sup>, Chang-Nan Chen<sup>1\*</sup> , Dinesh Chandra Agrawal<sup>1,3</sup> and Tai-Huei Wei<sup>4</sup>

## Abstract

This study synthesized a facile and high sensitive fluorescent probe based on sulfur-doped carbon dots (S-CDs) using a one-step microwave irradiation method. The probe exhibited a strong blue emission and a high quantum yield (QY) of 36.40%. In the detection, the presence of trivalent chromium (Cr(III)) strongly quenched the PL intensity of S-CDs by the inner filter effect (IFE) quenching mechanism of Cr(III) on the S-CDs. The S-CDs exhibited good sensitivity to turn-off Cr(III) detection with a linear range concentration of 0–45  $\mu\text{M}$  and a detection limit of 0.17  $\mu\text{M}$ . Furthermore, the proposed method has been successfully applied for Cr(III) detection in natural water samples with the 93.68–106.20% recoveries.

**Keywords:** Sulfur-doped carbon dots, Microwave irradiation, Trivalent chromium

## Introduction

Carbon dots (CDs) are carbon-based nanoparticles that have unique photoluminescent properties such as high photostability (Zhi et al. 2018), good solubility in water, easily modified with specific functional groups for various field applications (Karakoti et al. 2015; Farshbaf et al. 2018). In addition, CDs provide superior prospects both in cost-effectiveness and environmental friendliness (Pudza et al. 2020). Currently, carbon dots applications have tremendous concerns, e.g., metal sensing (Chahal et al. 2020; Khan et al. 2017; Zhang et al. 2016), tunable photoluminescence (Zheng et al. 2020), biosensor (Madrakian et al. 2017; Zhang and Guo 2021), bio-imaging (Zan et al. 2018), bio-labeling (Liu et al. 2019), biomedicine (Shaikh et al. 2018), photocatalytic energy conversion (Fernando et al. 2015), and as nanocarriers for gene delivery (Zuo et al. 2015). In metal sensing, carbon dots can detect metal by quenching or turning it off. This

causes a decrease in the intensity of PL carbon dots on the addition of metal (Khan et al. 2017).

The method for synthesizing carbon dots is generally divided into top-down and bottom-up (Zuo et al. 2015). Synthesis of carbon dots by breaking down large particles into nanoparticle-sized particles is called the top-down method, like oxidation (Misra et al. 2018; Tan et al. 2019), electrochemical (Ahirwar et al. 2017), laser ablation (Thongpool et al. 2012; Kang et al. 2020). In contrast, the bottom-up method is a method of arranging atoms or molecules to form the desired nanometer-sized particles like hydrothermal (Chahal et al. 2020), solvothermal (Zheng et al. 2020), pyrolysis (Li et al. 2020), microwave, and sonochemical assisted (Ashritha et al. 2021). The microwave method is a common bottom-up method for synthetic CDs due to being simple, fast, cost-efficient, and environmentally friendly (Ang et al. 2020). This method works by vibrating the carbon chain to undergo rearrangement (Guan et al. 2020).

This work synthesized carbon dots from succinic acid and sodium thiosulfate using a one-step microwave irradiation method. Succinic acid and sodium thiosulfates are biocompatible carbon and oxygen-rich

\*Correspondence: cnchen@cyut.edu.tw

<sup>1</sup> Department of Applied Chemistry, Chaoyang University of Technology, Taichung, Taiwan

Full list of author information is available at the end of the article

building blocks in chemical synthesis (Prathumsuwan et al. 2018). Succinic acid comprises mainly the carboxylic functionalize group and can be produced from *Actinobacillus succinogenes* through Broth fermentation (Lin et al. 2010). Meanwhile, Sulfur (S) is often used to improve the properties of optical carbon dots because of the similar electronegativity with carbon but a larger atomic radius than a carbon atom. Six valence electrons in each S atom can modify the electronic structure of CDs. Under certain conditions, zero-length bonds can be formed between the CDs and the target biomolecules from the disulfide covalent bonds (Karakoti et al. 2015). Therefore, the presence of S together with carboxylic acid functionality made S-CDs negatively charged and bright blue luminescent (Ding et al. 2020). The purpose of this study is to identify whether the naturally present functional groups in succinic acid's precursor and S will impact the optical properties of CDs and their sensing applications for presenting Cr(III) in water.

In surface water, the ratio of Cr(III) to hexavalent chromium varies widely. Generally, Cr(III) is a positive ion that forms hydroxides and complexes. Approximately 25% of Cr(III) of the available daily intake (2–8 g) is absorbed for metabolism, but Cr(III) compounds are cytotoxic. They might cause chromosomal damage in enormous amounts (Tumolo et al. 2020). Thus, selective and sensitive determination of chromium is important. Several methods have been used to detect Cr(III) in water, such as inductively coupled plasma atomic emission spectrometry (ICP-AES) (Liang et al. 2003), flame atomic absorption spectrometry (EAAS) (Sperling et al. 1992), X-ray fluorescence spectrometry (Inui et al. 2011) and electrochemical methods (Prabhakaran et al. 2020). However, several of these methods requires expensive costs and a complex procedure because the sample must be pre-treated, so that it takes a long time and is less efficient if applied. In addition, the method of using a colorimetric method based on nanoparticles has also been developed for a long time. One example is the synthesis of gold nanoparticles functionalized with mercaptobenzoic acid (Zhang et al. 2020). However, this nanoparticle is a bit tough to synthesize, so that a better method is needed.

Therefore, the synthesis of S-CDs from succinic acid as a precursor and sodium thiosulfate as an S source is an excellent alternative method for detecting Cr(III). Cr(III) is considered as a quencher for the mechanism of S-CDs fluorescence via IFE. In IFE, the quencher absorption spectrum overlaps with the CDs' excitation and/or emission (Lee et al. 2020; Tan et al. 2020; Panigrahi and Mishra 2019).

## Methods

### Materials

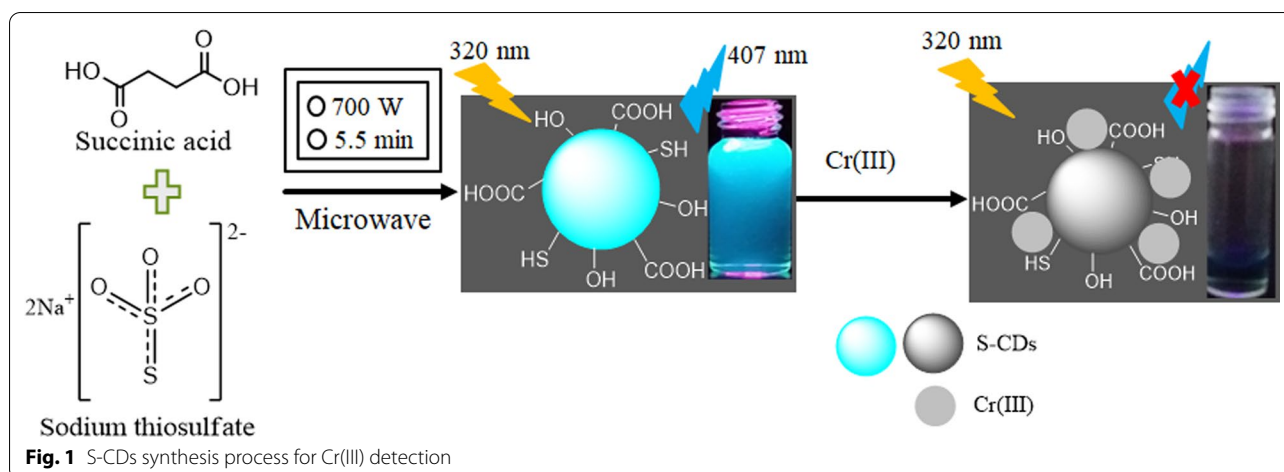
All chemicals were of analytical grade. Succinic acid ( $C_4H_6O_4$ ), quinine hemisulfate salt monohydrate ( $C_{40}H_{52}N_4O_9S$ ), lead(II) nitrate ( $Pb(NO_3)_2$ ), rubidium chloride (RbCl), and cesium chloride (CsCl) were obtained from Sigma-Aldrich (USA). Chromium(III) nitrate nonahydrate ( $Cr(NO_3)_3 \cdot 9H_2O$ ) was purchased from Alfa Aesar (USA). Nickel(II) nitrate hexahydrate ( $Ni(NO_3)_2 \cdot 6H_2O$ ) and magnesium nitrate hexahydrate ( $Mg(NO_3)_2 \cdot 6H_2O$ ) were procured from Showa (Japan). Sodium thiosulfate pentahydrate ( $Na_2S_2O_3 \cdot 5H_2O$ ) was purchased from Shimakyu's pure chemicals (Japan) and copper(II) sulfate pentahydrate ( $CuSO_4 \cdot 5H_2O$ ) was purchased from Choneye pure chemicals. Sodium hydroxide (NaOH) was purchased from Honeywell Fluka (Germany). Iron(II) chloride tetrahydrate ( $FeCl_2 \cdot 4H_2O$ ) and other metals were purchased from Merck (USA). Ultrapure water was obtained from a Milli-Q Reference purification system (18.2 M $\Omega$  cm, 25 °C).

### Synthesis of the S-CDs

The S-CDs were synthesized by microwave irradiation method according to previous reported method with small modification (Nemati et al. 2018a). Typically, succinic acid (0.5 g) and sodium thiosulfate (0.35 g) were dissolved with deionized water (15 mL) in crucible porcelain 50 mL. A domestic microwave irradiated the mixture solution at 700 W for 5.5 min. After irradiation, the resulting solid was dissolved in 10 mL for further centrifugation at 10,000 rpm for 30 min. This step is purposed to remove the insoluble material of S-CDs. The obtained supernatant was filtered by a micropore membrane filter (0.22  $\mu$ m). Thus, the solution containing S-CDs was kept for further analysis. The synthesis of S-CDs and their application as turn-off sensor for Cr(III) is depicted in Fig. 1.

### Characterization of S-CDs

S-CDs morphology was performed by transmission electron microscopy (TEM) on a JEOL JEM-2010 with an accelerating voltage of 200 kV. The surface of S-CDs was characterized by attenuated total reflectance-Fourier transform infrared (ATR-FTIR) spectrometer (Perkin Elmer, USA). PHI Hybrid Quantera conducted X-ray photoelectron spectroscopy (XPS) measurement. Characterization of the nature of the material was conducted by x-ray diffraction (XRD). The PL spectra were observed by FP-750 Spectrofluorometer (Jasco, Japan). All measurements were performed in 10 mm quartz microcells, at room temperature. Ultraviolet-visible



(UV–Vis) absorption spectra were obtained with Spectrophotometer Lambda 265 (Perkin Elmer, USA).

#### Measurement of quantum yield

The QY of synthesized S-CDs was measured by plotting the absorbance versus PL intensity of both S-CDs and quinine sulfate in 0.1 M  $H_2SO_4$  (QY = 0.54) as reference. The excitation wavelength was conducted at 320 nm and the QY calculation refers to the QY equation (Xu et al. 2020) based on Eq. (1):

$$QY_s = QY_r \frac{I_s A_r \eta_s^2}{I_r A_s \eta_r^2} \quad (1)$$

subscripts “s” and “r” stand for sulfur-doped carbon dots and reference quinine sulfate, respectively. “I” corresponds to the integrated PL intensity, “A” corresponds to the absorbance measured at the excited wavelength and “ $\eta$ ” refers to the solvent refractive index.

#### Sensitivity and selectivity of Cr(III)

To evaluate the range detection of S-CDs towards Cr(III), the series of Cr(III) concentration were mixed with 10  $\mu$ L S-CDs solution (0.02 mg/mL), respectively. Then, the mixture solution was diluted to 3 mL with deionized water. The solution was mixed thoroughly and kept at room temperature for 5 min. Afterward, the PL intensity was measured at excitation wavelength 320 nm and emission wavelength 407 nm. To describe the PL quenching profile of S-CDs with Cr(III) presence, the plot of  $I_0/I$  versus C was performed according to the Stern–Volmer equation (Ghanem et al. 2020) based on Eq. (2):

$$\frac{I_0}{I} = 1 + K_{SV}[C] \quad (2)$$

where  $I_0$  refers to the initial PL intensity,  $I$  represents the PL intensity with the presence of Cr(III),  $K_{SV}$  denotes the Stern–Volmer quenching constant, and  $C$  refers to the added concentration of metal ions.

To assess selectivity, different kinds of metal ions, e.g. Cr(III), Cs(I), K(I), Li(I), Mn(II), Na(I), Rb(I), Hg(II), Se(IV), Ni(II), Pb(II) and Fe(III) were tested with the S-CDs. 10  $\mu$ L S-CDs (0.02 mg/mL) and 60  $\mu$ L of metal ion (0.01 M) was transferred to vial, respectively. Then, the mixture solution was diluted to 3 mL with deionized water. The solution was mixed thoroughly and left to react at room temperature for 5 min, and then recorded the associated PL intensity. To validate the feasibility of S-CDs under environmental conditions, the S-CDs were applied in Taichung city in two different water samples (river water and tap water). A 0.22  $\mu$ m syringe filter filtered the water sample to reduce the insoluble materials and each sample (1 mL) was spiked with a known concentration of Cr(III) and S-CDs 10  $\mu$ L (0.02 mg/mL).

## Result and discussions

### Optimization of S-CDs synthesis

The synthesis of S-CDs was conducted by a microwave irradiation method using succinic acid as precursor and sodium thiosulfate as sulfur sources. The S-CDs synthesized has good solubility in water. A factorial design using three factors and two levels has been done to produce the S-CDs with the highest quantum yield and good optical properties. These factors are microwave power, time irradiation, and the amount of sodium thiosulfate, while succinic acid was 0.22 g for each experiment. The QY was determined by a plot of integrated PL intensity versus the absorbance of S-CDs and quinine sulfate (Additional file 2: Fig. S1). Quinine sulfate was used as fluorescent

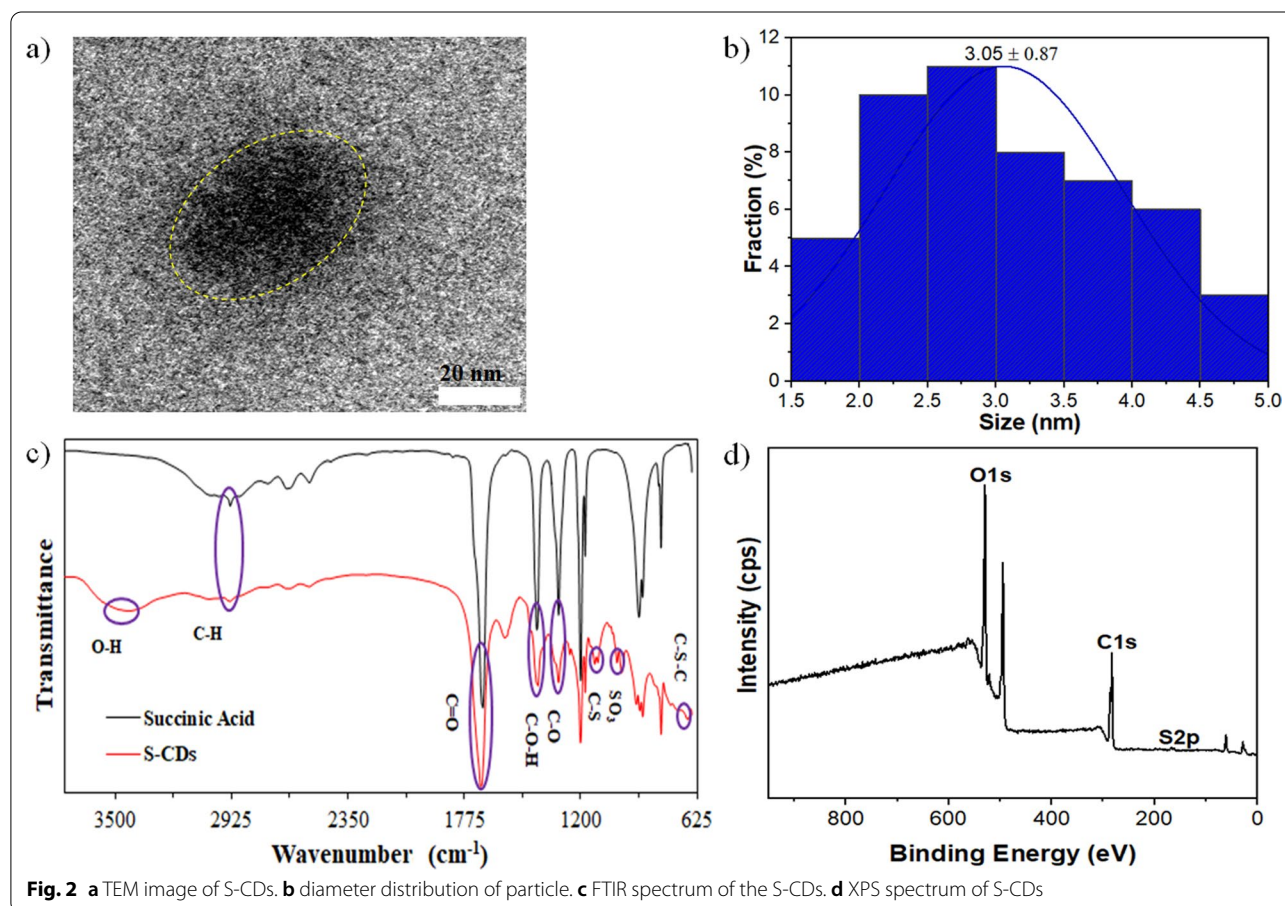
standard due to similar PL excitation and emission wavelength with the S-CDs synthesized. Thus, the highest QY for S-CDs was obtained 36.40% at the microwave power 700 W, the time irradiation 5.5 min and the amount of sodium thiosulfate 0.35 g (Additional file 1: Table S1). The microwave irradiation method provides an effective, efficient, and convenient method for synthesizing S-CDs. The microwave method could increase the particle size uniformity of carbon dots (Lin et al. 2019). Particle size could be attributed to the change rate of non-radiative radiation and relaxation mechanisms. Wherein an increase in particle size causes a decrease in quantum efficiency (Dijken et al. 2001). In addition, adding S as surface passivation can increase the QY due to its catalytic ability on the surface of S-CDs (Lin et al. 2019).

### S-CDs characterization

TEM image of synthesized S-CDs is displayed in Fig. 2a. The result showed that S-CDs were spherical in shape and distributed within the range of 1.5–5.0 nm (Fig. 2b). The XRD spectra indicated the degree of crystallinity of the S-CDs synthesized showed sharp peaks around 25.47°–28.06°. These peaks correspond

to graphite's (002) plan (Nemati et al. 2018a; Wang et al. 2019; Pakhira et al. 2016). The other sharp peak appeared at 13.93° and broad peaks appeared at 18.12° and 23.56°, which indicated highly disorder carbon atoms and confirmed the amorphous nature of carbon dots (Du et al. 2014; Bian et al. 2018). Thus, the synthesized S-CDs contained a structure of carbon, both crystalline and amorphous phases.

The FTIR spectra (Fig. 2c) presented the surface functionalities of S-CDs corresponding to succinic acid. Both the S-CDs and succinic acid were similar functional peaks, except the absorption peak at 665  $\text{cm}^{-1}$  in the S-CDs demonstrated C–S/C–S–C bending (Ouyang et al. 2019; Nemati et al. 2018a; Gupta and Nandi 2017). In addition, the peaks at 1122  $\text{cm}^{-1}$  and 1051  $\text{cm}^{-1}$  could be described as C–S and present of  $\text{SO}_3$ , respectively (Sun et al. 2016; Ding et al. 2014). Meanwhile, the peaks at 3430  $\text{cm}^{-1}$  and 2933  $\text{cm}^{-1}$  attributed to the broad absorption of O–H and C–H stretching vibration, respectively (Başoğlu et al. 2020; Lin et al. 2019). The peak of C=O representing carboxylic acid, and the C–O stretching vibration was indicated at 1692  $\text{cm}^{-1}$  at 1309  $\text{cm}^{-1}$  (Chandra et al. 2013). The peak at 1411  $\text{cm}^{-1}$



demonstrated C–O–H in-plane blending (Mitra et al. 2013). The FTIR spectra indicated that succinic precursors doped with S could be successfully prepared by microwave method.

The three peaks in the XPS spectrum characterized by C1s, O1s, and S2p, respectively, indicate that C, O, and S contained atomic percentage ratio of C:O:S=62.3:36.2:1.5 in the S-CDs synthesis (Fig. 2d). The high-resolution of XPS spectra showed the C1s spectrum at 284.5 assigned to C–C/C=C and the subsequent peaks at 285.5, 286.3, and 288.3 eV (Additional file 3: Fig. S2a) assigned to C–OH (hydroxyl), C–S, and C=O (carboxyl), respectively (Nemati et al. 2018b; Chandra et al. 2013). The two peaks at 532.1 and 535.6 eV in the O1s spectrum assigned C=O/COOH groups and OH (Additional file 3: Fig S2b). According to Fig. S2c, there were two main peaks of the S2p spectrum centered at 163.7 and 168.8 eV. The first centered peaks at 163.2 and 164.3 eV could be associated with 2p<sub>3/2</sub> and 2p<sub>1/2</sub> of the –C–S– covalent bond due to their spin–orbit couplings (Ding et al. 2014; Nemati et al. 2018b). The next peak could be deconvoluted into three peaks at 167.6, 168.5, and 169.3 eV, refer to the –C–SO<sub>x</sub>– (x=2, 3, 4) species (Ding et al. 2014; Gupta and Nandi 2017). Therefore, The FTIR and XPS approved the presence of C–C/C=C, C=O, –OH, –COOH, C–S, and C–SO<sub>x</sub> surface functional group in the S-CDs synthesis.

### Optical properties

The optical properties of S-CDs were conducted by UV–Vis and fluorescence techniques. As shown in Fig. 3a,

there were two unique absorption peaks of the S-CDs spectrum. The peak at 255 nm corresponded to  $\pi$ – $\pi^*$  transition of C=C, and the peak 320 nm corresponded to  $n \rightarrow \pi^*$  transition of C=O (Ouyang et al. 2019; Nemati et al. 2018c; Başoğlu et al. 2020). Under a 365 UV lamp, the S-CDs solution emitted a blue color (Fig. 3a inset). Figure 3b shows the photoluminescence (PL) emission spectra of S-CDs dependent on the excitation wavelength. There were two regions of fluorescence emitted according to fluorescence excitation. When the fluorescence excited from 300 to 340, the fluorescence emission displayed a red shift from 405 to 414 nm. Meanwhile, the fluorescence emission demonstrated a red shift from 446 to 504 nm when the fluorescence excitation was 350–480. Then, the fluorescence emission-dependent excitation wavelength resulted in the highest emission at 407 nm upon excitation by 320, giving rise to a blue emission. This color is due to the S doping of the CDs (Ding et al. 2014). Otherwise, the lowest emission at 504 nm upon excitation by wavelength 480 nm. Furthermore, there is no fluorescence emitted at fluorescence excited more than 480 nm.

The changing of emission wavelengths at different excitation wavelengths was related to functional groups on the surface, and the various sizes of S-CD particles (Lin et al. 2019; Jayaweera et al. 2019). The S is the one that has a strong electron affinity, which causes the increase in electron density in the intrinsic state of the S-CDs (Kang et al. 2020). The surface functional group of the S-CDs will act as an emission trap. The electronic structure of the carbon dots might be modulated by S

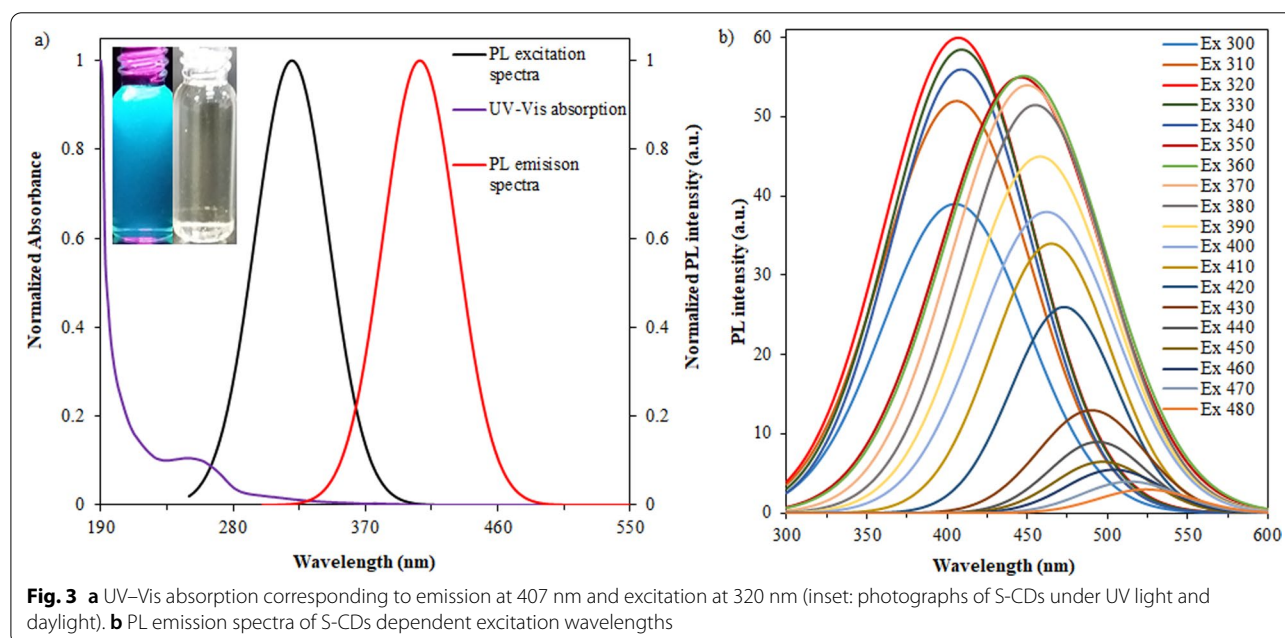


**Fig. 3** **a** UV–Vis absorption corresponding to emission at 407 nm and excitation at 320 nm (inset: photographs of S-CDs under UV light and daylight). **b** PL emission spectra of S-CDs dependent excitation wavelengths

through inputting the S energy levels between  $\pi$  and  $\pi^*$  of carbon to produce multi-emission peaks (Feng et al. 2018). In addition, different functional groups provide different energy levels. It was possible due to the ability of each functional group to supply electrons to the CDs. On the other hand, the change in S-CD particle size resulted in a localized state associated with discrete  $sp^2$  at the Lowest Unoccupied Molecular Orbital (LUMO) and Highest Occupied Molecular Orbital (HOMO) levels (Ouyang et al. 2019; Kang et al. 2020). When the particles get smaller, there was a larger energy gap between the 2 levels, which caused the electrons in the HOMO to need more a lot of energy to get excited into the LUMO. The electronic transitions in these localized states were responsible for the redshift of the fluorescence emission wavelength (Ouyang et al. 2019; Feng et al. 2018).

#### Photostability of the S-CDs

Four critical factors were observed to evaluate the stability of the S-CDs. These were: the effect of various ionic strength concentrations, different temperatures, different time exposure to ultraviolet light (under UV light 365 nm), and the effect of various pH. The effect of ionic strength on PL intensity was studied with a range concentration of NaCl solution from 0 to 200 mM. The PL intensity was stable even at high NaCl concentration (Additional file 4: Fig. S3a), which indicated the high colloid stability possessed by S-CDs against the attractive forces of the particles (Jayaweera et al. 2019; Nemati et al. 2018c). This showed that the PL intensity was independent of ionic strength. Under environmental conditions, the PL intensity remained unchanged because the primary mechanism was not disturbed by the presence of ions. In contrast, increasing temperatures resulted in a decrease in PL intensity (Additional file 4: Fig. S3b). Increased temperature indicates diminishing fluorescence caused by non-radiant heat, leading to reduced radiation emissions.

To ensure photostability of S-CDs was conducted by continuous UV irradiation using UV light 365 nm for 120 min. Additional file 4: Fig. S3c demonstrated a decrease in PL intensity after 60 min and 120 min of exposure by 14% and 21%, respectively. In traditional fluorescent dyes such as Rhodamine 6G, the reduction in PL intensity after 120 min of continuous exposure was almost 54% (Madjene et al. 2021). This shows that the S-CDs were more resistant to photobleaching. Furthermore, to determine the effect of pH on PL intensity, it was carried out in the pH value from 1 to 12. The most vigorous PL intensity occurred at pH 3 (Additional file 4: Fig. S3d). An increase in pH value resulted in a decrease in PL intensity, but an increase in PL intensity returned to pH 6. A similar pattern occurred in the pH between

6 and 10. The pH-dependent PL intensity was related to the protonation/deprotonation of the carboxyl ( $-\text{COOH}$ ) and hydroxyl groups ( $-\text{OH}$ ) on the S-CD surface (Huang et al. 2015). Therefore, the unique PL intensity characteristics as a function of pH provided a good direction for determining metal ions, especially in acidic environments (Issa et al. 2020).

#### Sensitivity and selectivity of S-CDs towards Cr(III)

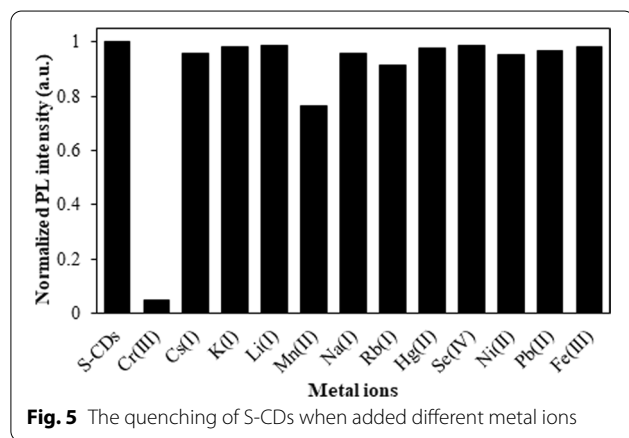
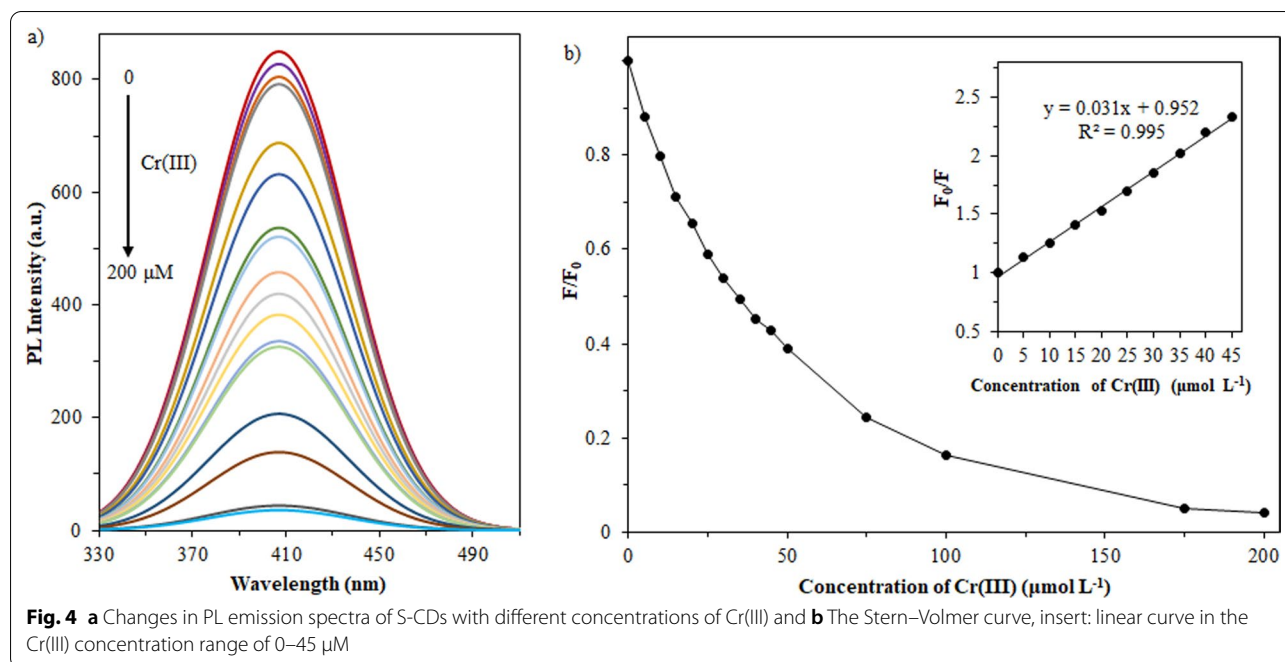
The fluorescence quenching refers to Stern–Volmer, which is expressed by Eq. 2. While the limit of detection was calculated using  $3\delta/m$ , where the standard deviation of the blank signal was denoted by  $\delta$  and  $m$  refers to the slope of the linear correlation. As shown in Fig. 4a, the S-CDs' PL intensity demonstrated a significant decrease with the increasing concentration of Cr(III) from 0 to 200  $\mu\text{M}$  compared to the other metal ions. A good linear correlation ( $R^2$ , 0.995) was showed between quenching efficiency  $I_0/I$  and concentration Cr(III) in a range of 0–45  $\mu\text{M}$  (Fig. 4b), and the limit of detection (LOD) was calculated to be 0.17  $\mu\text{M}$ .

Several metal ions were prepared to evaluate the selectivity of S-CDs towards Cr(III). These ions included Cr(III), Na(I), Li(I), Cs(I), K(I), Mn(II), Rb(I), Hg(II), Se(IV), Ni(II), Pb(II) and Fe(III) with a concentration of 200  $\mu\text{M}$  for each ion and they were tested with 10  $\mu\text{l}$  S-CDs solution (0.02 mg/mL). Figure 5 shows the PL intensity was quenched by the presence of Cr(III), about 95% of the initial PL intensity of S-CDs. These results confirmed that the S-CDs have high selectivity towards Cr(III) compared to other metals.

Table 1 shows the comparison between the feasibility of Cr(III) detection in this study and other related results, including linear detection range and LOD.

#### Possible mechanism of Cr(III) detection

To evaluate the quenching mechanism by Cr(III), the absorbance spectra of the presence of Cr(III) with S-CDs were matched with PL excitation spectra and PL emission spectra from S-CDs (Fig. 6a). There was a good spectral overlap in the excitation and emission of S-CDs with the absorption spectrum of Cr(III). This phenomenon could occur through the IFE process due to the overlap of the quencher absorption spectrum with excitation called the primary inner-filter effect and/or the emission of CDs called the secondary inner-filter effect (Lee et al. 2020; Tan et al. 2020; Panigrahi and Mishra 2019). Thus, IFE involved primary and secondary quenching mechanisms on the S-CDs surface in the presence of Cr(III). IFE was considered the quenching fluorescence mechanism rather than the fluorescence resonant energy transfer process due to the excellent overlap between the quencher absorption spectrum and CDs' excitation

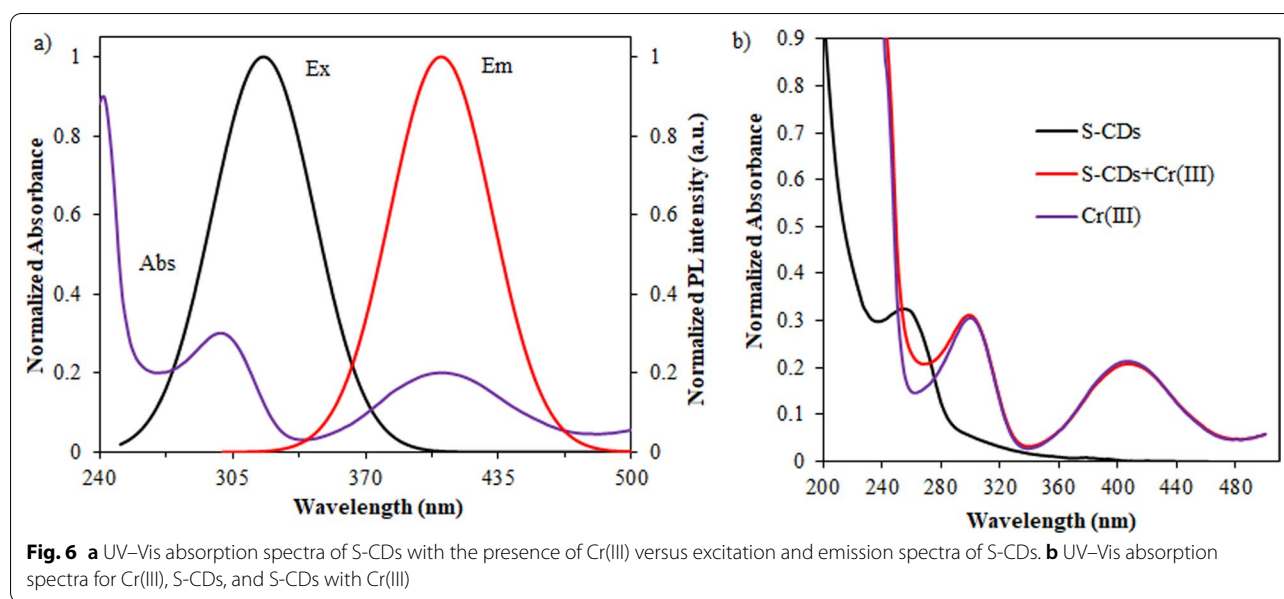


and emission spectra (Zhao et al. 2018; Al-Hashimi et al. 2020). The PL intensity of S-CDs was reduced by adding Cr(III) to the S-CDs solution. In this phenomenon, Cr(III) would absorb the emission light of S-CDs, but the excitation light would be constant since the addition of Cr(III) into the S-CDs solution. Therefore, the emission PL intensity of S-CDs would be a turn-off (Shahbazi and Zare-Dorabei 2019; Mousavi et al. 2020). Figure 6b shows no difference in absorption spectrum S-CDs both in absence Cr(III) and presence Cr(III). This confirmed the impossibility of forming the ground-state complex between S-CDs and Cr(III).

Based on energy perspective, the band gaps values between S-CDs and S-CDs with Cr(III) were calculated

**Table 1** Comparison of different sensing methods for detection of Cr(III)

Detection probe	Linear range (μM)	LOD (μM)	Refs.
AuNPs modified 4-mercaptobenzoic acid	20–25	5	Zhang et al. (2020)
Au NPs unmodified	0.1–1	0.1	Elavarasi et al. (2014)
Rhodamine modified polyamidoamine dendrimer	10–100	10	Lei et al. (2011)
Au NPs functionalized triazole	5–65	1.4	Chen et al. (2013)
Benzimidazole-based imine-linked	79.4–340	79.4	Saluja et al. (2012)
γ-CDs	0–200	24.58	Chang et al. (2016)
DDCDs	0.1–6	0.027	Lu et al. (2019)
Cu-CDs	5–150	0.12	Li et al. (2021)
OCDs	1–96	0.38	Si et al. (2021)
S-CDs	0–45	0.17	This work

**Table 2** Cr(III) detection in water samples (n = 3)

Sample	Spiked concentration (μmol/L)	Measured concentration (μmol/L)	Recovery (%)	RSD (%)
Tap water	5.00	5.76	104.45	0.21
	10.00	9.96	94.74	0.52
	15.00	14.72	94.86	0.45
River water	5.00	5.59	106.20	0.20
	10.00	9.62	93.68	0.74
	15.00	15.05	98.65	0.32

using the Tauc plot equation (Aziz et al. 2019) as formulated in Eq. 3:

$$(\alpha h\nu) = k(h\nu - E_g)^\gamma \quad (3)$$

where  $h\nu$  is the photon energy,  $\alpha$  is coefficient of absorption,  $E_g$  is the band gap,  $\gamma$  is the index for the responsible electronic transition ( $\alpha h\nu$ )<sup>2</sup> indicated a direct allowed electron transition of  $\frac{1}{2}$ , and  $k$  is the parameter dependent on the inter-band transition. As shown by Additional file 5: Fig. S4a and S4b, Cr(III) in S-CDs indicated a reduction in band gap energy. S-CDs' absorption causes the absorption edge to shift in the direction of low photon energy (Aziz et al. 2019). In addition, the lower band gap was related to the charge of metal ions on the surface of CDs (Murugan et al. 2019).

#### Application of S-CDs on water samples for Cr(III) detection

Experiments in two water sources were carried out to investigate the visibility of S-CDs for Cr(III) detection. Three known concentrations of Cr(III) were respectively introduced to the water sample. The results showed an increase in the concentration of Cr(III) quenched on the PL intensity of each water sample. As shown in Table 2, the percentage of water sample recovery is in the range of 93.68–106.20, while the relative standard deviation (RSD) ranges from 0.20 to 0.74. These results support that S-CDs have the feasibility of being applied as a sensor to detect Cr(III) in water in actual environmental conditions.

#### Conclusion

In summary, we have developed the water-soluble S-CDs fluorescent sensor to detect Cr(III) in water samples. A microwave irradiation method was adopted to prepare S-CDs using succinic acid as a precursor, and sodium thiosulfate as a source of S. The PL intensity of S-CDs was effectively quenched by the presence of Cr(III) due to the IFE of Cr(III) on S-CDs. Therefore, the proposed method was successfully used to detect Cr(III) in actual water samples, which can be considered for analyzing Cr(III) in other samples. Our present work provides the advantage of simplicity, saving time, low cost, and selectivity.



## Abbreviations

S-CDs: Sulfur-doped carbon dots; PL: Photoluminescence; Cr(III): Trivalent chromium; IFE: Inner filter effect; CDs: Carbon dots; S: Sulfur; ICP-AES: Inductively coupled plasma atomic emission spectrometry; EAAS: Flame atomic absorption spectrometry; ATR-FTIR: Attenuated total reflectance-Fourier transform infrared; XRD: X-ray diffraction; UV-Vis: Ultraviolet-visible; QY: Quantum yield; LOD: Limit of detection; RSD: Relative standard deviation.

## Supplementary Information

The online version contains supplementary material available at <https://doi.org/10.1186/s40543-021-00298-y>.

**Additional file 1. Table S1.** The quantum yield (%) for synthesis S-CDs based on a factorial design of three factors and two levels ( $2^3$ ).

**Additional file 2. Fig. S1.** Integrated PL Intensity versus Absorbance for quinine sulfate and S-CDs.

**Additional file 3. Fig. S2.** High-resolution XPS spectra **a** C1s, **b** O1s, and **c** S2p.

**Additional file 4. Fig. S3.** Photostability of S-CDs at excitation wavelength 320 nm under **a** continuous of UV irradiation, **b** various chloride concentration, **c** various temperature and **d** various pH.

**Additional file 5. Fig. S4.** **a** Band gap of S-CDs and **b** Band gap of S-CDs with Cr(III).

## Acknowledgements

The first author (SRK) gratefully acknowledges the Analytical Chemistry Laboratory, Department of Applied Chemistry, Chaoyang University of Technology (CYUT), to facilitate this research. Also, the first author would like to thank CYUT for a doctoral fellowship and be grateful for the support from the Institute of Educational Development-West Nusa Tenggara (LPP-NTB), Indonesia. All the authors especially thank the Instruments Center at National Chung Cheng University, Chiayi, Taiwan for supporting TEM and XPS measurements.

## Authors' contributions

SRK and CNC designed the concept and the experiment method of the research. SRK carried out the experiments, collected and analyzed data, and wrote the first draft of the manuscript. CNC supervised the study and reviewed the manuscript. DCA revised the manuscript and provided substantial inputs to the manuscript. THW made valuable contributions to TEM and XPS characterization. All authors have read and agreed to the published version of the manuscript.

## Funding

Not applicable.

## Availability of data and materials

All data generated and analyzed in this study have been provided in the manuscript.

## Declarations

### Competing interests

The authors declare that they have no competing interests.

### Author details

<sup>1</sup>Department of Applied Chemistry, Chaoyang University of Technology, Taichung, Taiwan. <sup>2</sup>Department of Environmental Science, University of Mataram, Mataram, Indonesia. <sup>3</sup>Department of Environmental Engineering and Management, Chaoyang University of Technology, Taichung, Taiwan. <sup>4</sup>Department of Physics, National Chung Cheng University, Chiayi, Taiwan.

Received: 7 June 2021 Accepted: 3 October 2021

Published online: 26 October 2021

## References

- Ahirwar S, Mallick S, Bahadur D. Electrochemical method to prepare graphene quantum dots and graphene oxide quantum dots. *ACS Omega*. 2017;2:8343–53.
- Al-Hashimi B, Rahman HS, Omer KM. Highly luminescent and biocompatible P and N Co-doped passivated carbon nanodots for the sensitive and selective determination of rifampicin using the inner filter effect. *Materials (basel)*. 2020;13:2275.
- Ang WL, Boon Mee CAL, Sambudi NS, Mohammad AW, Leo CP, Mahmoudi E, Ba-Abbad M, Benamor A. Microwave-assisted conversion of palm kernel shell biomass waste to photoluminescent carbon dots. *Sci Rep*. 2020;10:1–15.
- Ashritha MG, Rondiya SR, Cross RW, Dzade NY, Dhole SD, Hareesh K, Sunitha DV. Experimental and computational studies of sonochemical assisted anchoring of carbon quantum dots on reduced graphene oxide sheets towards the photocatalytic activity. *Appl Surf Sci*. 2021;545:148962.
- Aziz SB, Abdullah OG, Brza MA, Azawy AK, Tahir DA. Effect of carbon nano-dots (CNDs) on structural and optical properties of PMMA polymer composite. *Results Phys*. 2019;15:102776.
- Başoğlu A, Ocak Ü, Gümrükçüoğlu A. Synthesis of microwave-assisted fluorescence carbon quantum dots using roasted-chickpeas and its applications for sensitive and selective detection of Fe<sup>3+</sup> ions. *J Fluoresc*. 2020;30:515–26.
- Bian W, Wang X, Wang Y, Yang H, Huang J, Cai Z, Choi MMF. Boron and nitrogen co-doped carbon dots as a sensitive fluorescent probe for the detection of curcumin. *Luminescence*. 2018;33:174–80.
- Chahal S, Yousefi N, Tufenkji N. Green synthesis of high quantum yield carbon dots from phenylalanine and citric acid: role of stoichiometry and nitrogen doping. *ACS Sustain Chem Eng*. 2020;8:5566–75.
- Chandra S, Patra P, Pathan SH, Roy S, Mitra S, Layek A, Bhar R, Pramanik P, Goswami A. Luminescent S-doped carbon dots: an emergent architecture for multimodal applications. *J Mater Chem B*. 2013;1:2375–82.
- Chang MMF, Ginjom IR, Ngu-Schwemlein M, Ng SM. Synthesis of yellow fluorescent carbon dots and their application to the determination of chromium(III) with selectivity improved by pH tuning. *Microchim Acta*. 2016;183:1899–907.
- Chen YC, Lee IL, Sung YM, Wu SP. Triazole functionalized gold nanoparticles for colorimetric Cr<sup>3+</sup> sensing. *Sensors Actuators B Chem*. 2013;188:354–9.
- Dijken AV, Makkinje J, Meijerink A. The influence of particle size on the luminescence quantum efficiency of nanocrystalline ZnO particles. *J Lumin*. 2001;92:323–8.
- Ding H, Li XH, Chen XB, Wei JS, Li XB, Xiong HM. Surface states of carbon dots and their influences on luminescence. *J Appl Phys*. 2020;127:231101.
- Ding H, Wei JS, Xiong HM. Nitrogen and sulfur co-doped carbon dots with strong blue luminescence. *Nanoscale*. 2014;6:13817–23.
- Du F, Zhang M, Li X, Li J, Jiang X, Li Z, et al. Economical and green synthesis of bagasse-derived fluorescent carbon dots for biomedical applications. *Nanotechnology*. 2014;25:315702.
- Elavarasi M, Alex SA, Chandrasekaran N, Mukherjee A. Simple fluorescence-based detection of Cr(III) and Cr(VI) using unmodified gold nanoparticles. *Anal Methods*. 2014;6:9554–60.
- Farshbaf M, Davaran S, Rahimi F, Annabi N, Salehi R, Akbarzadeh A. Carbon quantum dots: recent progresses on synthesis, surface modification and applications. *Artif Cells Nanomed Biotechnol*. 2018;46:1331–48.
- Feng J, Dong H, Pang B, Shao F, Zhang C, Yu L, Dong L. Theoretical study on the optical and electronic properties of graphene quantum dots doped with heteroatoms. *Phys Chem Chem Phys*. 2018;20:15244–52.
- Fernando KAS, Sahu S, Liu Y, Lewis WK, Gulians EA, Jafariyan A, Wang P, Bunker CE, Sun Y. Carbon quantum dots and applications in photocatalytic energy conversion. *ACS Appl Mater Interfaces*. 2015;7:8363–76.
- Ghanem A, Al-Qassar Bani Al-Marjeh R, Atassi Y. Novel nitrogen-doped carbon dots prepared under microwave-irradiation for highly sensitive detection of mercury ions. *Heliyon*. 2020;6:e03750.
- Guan C, Zhan L, Yang X, Dai G, Xiao Y. Significant effect of vibration treatment on microwave curing carbon fiber reinforced plastic. *J Reinf Plast Compos*. 2020;39:373–83.
- Gupta A, Nandi CK. PC12 live cell ultrasensitive neurotransmitter signaling using high quantum yield sulphur doped carbon dots and its extracellular Ca<sup>2+</sup> ion dependence. *Sensors Actuators, B Chem*. 2017;245:137–45.

- Huang L, Yang S, Chen L, Chen S. Hydrothermal synthesis of fluorescent carbon dots towards ion response and silk screen patterns. *Chem Lett*. 2015;44:1251–3.
- Inui T, Abe W, Kitano M, Nakamura T. Determination of Cr(III) and Cr(VI) in water by wavelength-dispersive X-ray fluorescence spectrometry after preconcentration with an ion-exchange resin disk. *X-Ray Spectrom*. 2011;40:301–5.
- Issa MA, Abidin ZZ, Sobri S, Rashid SA, Mahdi MA, Ibrahim NA. Fluorescent recognition of Fe<sup>3+</sup> in acidic environment by enhanced-quantum yield N-doped carbon dots: optimization of variables using central composite design. *Sci Rep*. 2020;10:1–19.
- Jayaweera S, Yin K, Ng WJ. Nitrogen-doped durian shell derived carbon dots for inner filter effect mediated sensing of tetracycline and fluorescent ink. *J Fluoresc*. 2019;29:221–9.
- Kang S, Jeong YK, Jung KH, Son Y, Kim WR, Ryu JH, Kim KM. One-step synthesis of sulfur-incorporated graphene quantum dots using pulsed laser ablation for enhancing optical properties. *Opt Express*. 2020;28:21659.
- Karakoti AS, Shukla R, Shanker R, Singh S. Surface functionalization of quantum dots for biological applications. *Adv Colloid Interface Sci*. 2015;215:28–45.
- Khan WU, Wang D, Zhang W, Tang Z, Ma X, Ding X, Du S, Wang Y. High quantum yield green-emitting carbon dots for Fe(III) detection, biocompatible fluorescent ink and cellular imaging. *Sci Rep*. 2017;7:1–9.
- Lee HJ, Jana J, Chung JS, Hur SH. Uncovering the actual inner-filter effect between highly efficient carbon dots and nitroaromatics. *Spectrochim Acta A Mol Biomol Spectrosc*. 2020;236:118342.
- Lei Y, Su Y, Huo J. A novel fluorescent sensor for Cr<sup>3+</sup> based on rhodamine-colored poly (amidoamine) dendrimer. *Spectrochim Acta A Mol Biomol Spectrosc*. 2011;83:149–54.
- Li Q, Yang D, Yang Y. Spectrofluorimetric determination of Cr(VI) and Cr(III) by quenching effect of Cr(III) based on the Cu-CDs with peroxidase-mimicking activity. *Spectrochim Acta A Mol Biomol Spectrosc*. 2021;244:118882.
- Li HW, Mao JY, Lien CW, Wang CK, Lai JY, Mandal RP, Chang HT, Chang L, Ma DHK, Huang CC. Platinum ions mediate the interactions between DNA and carbon quantum dots: diagnosis of MRSA infections. *J Mater Chem B*. 2020;8:3506–12.
- Liang P, Yang L, Hu B, Jiang Z. ICP-AES detection of ultratrace aluminum(III) and chromium(III) ions with a microcolumn preconcentration system using dynamically immobilized 8-hydroxyquinoline on TiO<sub>2</sub> nanoparticles. *Anal Sci*. 2003;19:1167–71.
- Lin SKC, Du C, Blaga AC, Camarut M, Webb C, Stevens CV, Soetaert W. Novel resin-based vacuum distillation-crystallisation method for recovery of succinic acid crystals from fermentation broths. *Green Chem*. 2010;12:666–7.
- Lin H, Huang J, Ding L. Preparation of Carbon Dots with High-Fluorescence Quantum Yield and their Application in Dopamine Fluorescence Probe and Cellular Imaging. *J Nanomater*. 2019;2019:1–9.
- Liu Y, Jiang L, Li B, Fan X, Wang W, Liu P, Xu S, Luo X. Nitrogen doped carbon dots: Mechanism investigation and their application for label free CA125 analysis. *J Mater Chem B*. 2019;7:3053–8.
- Lu H, Xu S, Liu J. One Pot Generation of Blue and Red Carbon Dots in One Binary Solvent System for Dual Channel Detection of Cr<sup>3+</sup> and Pb<sup>2+</sup> Based on Ion Imprinted Fluorescence Polymers. *ACS Sensors*. 2019;4:1917–24.
- Madjene F, Assassi M, Chokri I, Enteghar T, Lebig H. Optimization of photocatalytic degradation of rhodamine B using Box-Behnken experimental design: Mineralization and mechanism. *Water Environ Res*. 2021;93:112–22.
- Madrakian T, Maleki S, Gilak S, Afkhami A. Turn-off fluorescence of amino-functionalized carbon quantum dots as effective fluorescent probes for determination of isotretinoin. *Sensors Actuators, B Chem*. 2017;247:428–35.
- Misra SK, Srivastava I, Khamo JS, Krishnamurthy VV, Sar D, Schwartz-Duval AS, Soares JANT, Zhang K, Pan D. Carbon dots with induced surface oxidation permits imaging at single-particle level for intracellular studies. *Nanoscale*. 2018;10:18510–9.
- Mitra T, Sailakshmi G, Gnanamani A, Mandal AB. Studies on cross-linking of succinic acid with chitosan/collagen. *Mater Res*. 2013;16:755–65.
- Mousavi A, Zare-Dorabei R, Mosavi SH. A novel hybrid fluorescence probe sensor based on metal-organic framework@carbon quantum dots for the highly selective detection of 6-mercaptopurine. *Anal Methods*. 2020;12:5397–406.
- Murugan N, Prakash M, Jayakumar M, Sundaramurthy A, Sundramoorthy AK. Green synthesis of fluorescent carbon quantum dots from Eleusine coracana and their application as a fluorescence 'turn-off' sensor probe for selective detection of Cu<sup>2+</sup>. *Appl Surf Sci*. 2019;476:468–80.
- Nemati F, Hosseini M, Zare-Dorabei R, Salehnia F, Ganjali MR. Fluorescent turn on sensing of Caffeine in food sample based on sulfur-doped carbon quantum dots and optimization of process parameters through response surface methodology. *Sensors Actuators, B Chem*. 2018a;273:25–34.
- Nemati F, Hosseini M, Zare-Dorabei R, Ganjali MR. Sensitive recognition of ethion in food samples using turn-on fluorescence N and S co-doped graphene quantum dots. *Anal Methods*. 2018b;10:1760–6.
- Nemati F, Zare-Dorabei R, Hosseini M, Ganjali MR. Fluorescence turn-on sensing of thiamine based on Arginine – functionalized graphene quantum dots (Arg-GQDs): Central composite design for process optimization. *Sensors Actuators, B Chem*. 2018c;255:2078–85.
- Ouyang Z, Lei Y, Chen Y, Zhang Z, Jiang Z, Hu J, Lin Y. Preparation and Specific Capacitance Properties of Sulfur, Nitrogen Co-Doped Graphene Quantum Dots. *Nanoscale Res Lett*. 2019;14:219.
- Pakhira B, Ghosh M, Allam A, Sarkar S. Carbon nano onions cross the blood brain barrier. *RSC Adv*. 2016;6:29779–82.
- Panigrahi SK, Mishra AK. Inner filter effect in fluorescence spectroscopy: as a problem and as a solution. *J Photochem Photobiol C Photochem Rev*. 2019;41:100318.
- Prabhakaran DC, Ramamurthy PC, Sivry Y, Subramanian S. Electrochemical detection of Cr(VI) and Cr(III) ions present in aqueous solutions using bio-modified carbon paste electrode: a voltammetric study. *Int J Environ Anal Chem*. 2020;00:1–21.
- Prathumsuwan T, Jamnongsong S, Sampattavanich S, Paoprasert P. Preparation of carbon dots from succinic acid and glycerol as ferrous ion and hydrogen peroxide dual-mode sensors and for cell imaging. *Opt Mater (amst)*. 2018;86:517–29.
- Pudza MY, Abidin ZZ, Rashid SA, Yasin FM, Noor ASM, Issa MA. Eco-friendly sustainable fluorescent carbon dots for the adsorption of heavy metal ions in aqueous environment. *Nanomaterials*. 2020;10:315.
- Saluja P, Sharma H, Kaur N, Singh N, Jang DO. Benzimidazole-based imine-linked chemosensor: Chromogenic sensor for Mg<sup>2+</sup> and fluorescent sensor for Cr<sup>3+</sup>. *Tetrahedron*. 2012;68:2289–93.
- Shahbazi N, Zare-Dorabei R. A novel "off-on" fluorescence nanosensor for sensitive determination of sulfide ions based on carbon quantum dots and gold nanoparticles: Central composite design optimization. *Microchem J*. 2019;145:996–1002.
- Shaikh AF, Tamboli MS, Patil RH, Bhan A, Ambekar JD, Kale BB. Bioinspired carbon quantum dots: an antibiofilm agents. *J Nanosci Nanotechnol*. 2018;19:2339–45.
- Si J, Wang H, Wu B, Wang G, Yang J, Huo Z, Tian T, Zhao X, Han S. Preparation of carbon dots with orange emission for Cr(III) detection and cellular imaging. *Micro Nano Lett*. 2021;16:58–63.
- Sperling M, Xu S, Welz B. Determination of chromium(III) and chromium(VI) in water using flow injection on-line preconcentration with selective adsorption on activated alumina and flame atomic absorption spectrometric detection. *Anal Chem*. 1992;64:3101–8.
- Sun C, Zhang Y, Wang P, Yang Y, Wang Y, Xu J, Yu WW. Synthesis of nitrogen and sulfur co-doped carbon dots from garlic for selective detection of Fe<sup>3+</sup>. *Nanoscale Res Lett*. 2016;11:1–9.
- Tan C, Zuo S, Zhao Y, Shen B. Preparation of multicolored carbon quantum dots using HNO<sub>3</sub>/HClO<sub>4</sub> oxidation of graphitized carbon. *J Mater Res*. 2019;1–11.
- Tan X, Zhang P, Ye C, Min Y, Li Q, Wang Y. Signal-on photoluminescent detection of dopamine with carbon dots-MnO<sub>2</sub> nanosheets platform based on inner filter effect. *Dye Pigment*. 2020;180:108515.
- Thongpool V, Asanithi P, Limsuwan P. Synthesis of carbon particles using laser ablation in ethanol. *Procedia Eng*. 2012;32:1054–60.
- Tumolo M, Ancona V, De Paola D, Losacco D, Campanale C, Massarelli C, Uricchio VF. Chromium pollution in European water, sources, health risk, and remediation strategies: An overview. *Int J Environ Res Public Health*. 2020;17:1–25.
- Wang T, Wang A, Wang R, Liu Z, Sun Y, Shan G, Chen Y, Liu Y. Carbon dots with molecular fluorescence and their application as a "turn-off" fluorescent probe for ferricyanide detection. *Sci Rep*. 2019;9:1–9.
- Xu S, Ye S, Xu Y, Liu F, Zhou Y, Yang Q, Peng H, Xiong H, Zhang Z. Microwave-assisted synthesis of n, s-co-carbon dots as switch-on fluorescent sensor for

- rapid and sensitive detection of ascorbic acid in processed fruit juice. *Anal Sci*. 2020;36:353–60.
- Zan M, Rao L, Huang H, Xie W, Zhu D, Li L, Qie X, Guo S, Zhao X, Liu W, Dong W. A strong green fluorescent nanoprobe for highly sensitive and selective detection of nitrite ions based on phosphorus and nitrogen co-doped carbon quantum dots. *Sensors Actuators B Chem*. 2018;262:555–61.
- Zhang HC, Guo YM. Advances of carbon quantum dots for fluorescence turn-on detection of reductive small biomolecules. *Chinese J Anal Chem*. 2021;49:14–23.
- Zhang Y, Cui P, Zhang F, Feng X, Wang Y, Yang Y, Liu X. Fluorescent probes for “off-on” highly sensitive detection of  $Hg^{2+}$  and L-cysteine based on nitrogen-doped carbon dots. *Talanta*. 2016;152:288–300.
- Zhang Z, Ye X, Liu Q, Liu Y, Liu R. Colorimetric detection of  $Cr^{3+}$  based on gold nanoparticles functionalized with 4-mercaptopbenzoic acid. *J Anal Sci Technol*. 2020;11:0–6.
- Zhao C, Jiao Y, Gao Z, Yang Y, Li H. N, S co-doped carbon dots for temperature probe and the detection of tetracycline based on the inner filter effect. *J Photochem Photobiol A Chem*. 2018;367:137–44.
- Zheng J, Xie Y, Wei Y, Yang Y, Liu X, Chen Y, Xu B. An efficient synthesis and photoelectric properties of green carbon quantum dots with high fluorescent quantum yield. *Nanomaterials*. 2020;10:1–15.
- Zhi B, Gallagher MJ, Frank BP, Lyons TY, Qiu TA, Da J, Mensch AC, Hamers RJ, Rosenzweig Z, Fairbrother DH, Haynes CL. Investigation of phosphorous doping effects on polymeric carbon dots: fluorescence, photostability, and environmental impact. *Carbon*. 2018;129:438–49.
- Zuo J, Jiang T, Zhao X, Xiong X, Xiao S, Zhu Z. Preparation and application of fluorescent carbon dots. *J Nanomater*. 2015;2015:1–13.

### Publisher's Note

Springer Nature remains neutral with regard to jurisdictional claims in published maps and institutional affiliations.

Submit your manuscript to a SpringerOpen<sup>®</sup> journal and benefit from:

- Convenient online submission
- Rigorous peer review
- Open access: articles freely available online
- High visibility within the field
- Retaining the copyright to your article

---

Submit your next manuscript at ► [springeropen.com](https://www.springeropen.com)

---